Int J Mech Mater Des (2008) 4:383–389
DOI 10.1007/s10999-008-9069-z

A traceable calibration procedure for MEMS-based load cells

Khawar Abbas · Zayd C. Leseman · Thomas J. Mackin

Received: 31 October 2007 / Accepted: 27 February 2008 / Published online: 15 March 2008

Abstract Characterizing the mechanical properties of materials and biological systems at the nanoscale requires accurate measurement of forces on the order of μN and less. Due to the scale of the measurements and size of the instrumentation, calibration of nanoscale devices presents a new challenge in metrology. In order to ensure accuracy of results, traceable calibrations must be performed on nanoscale instrumentation. Our group recently developed a novel MEMS-based high resolution load cell with force resolution on the order of μN. This paper reports on a simple method for traceably calibrating our device using dead weights that could be generalized to other MEMS-based load cells. In this article, fabrication of a MEMS load cell is detailed and we compare our calibrated force–displacement curves to a non-linear theoretical prediction, revealing errors as great as 29%.

Keywords Metrology · Calibration · MEMS · Load cell

K. Abbas · Z. C. Leseman (✉)
Department of Mechanical Engineering, The University of New Mexico, MSC01-1150, Albuquerque, NM 87131-0001, USA
e-mail: zleseman@unm.edu

T. J. Mackin
Department of Mechanical Engineering, Cal Poly, San Luis Obispo, CA, USA

1 Introduction

MEMS technology has enabled the development of novel load-cells with ultra-high force resolution (μN or less). Recent examples can be found in Onoe and Takeo (1998), Sun et al. (2003), Zhang (2004), Saif and McDonald (1998), Samuel et al. (2005), and others. Each of these researchers have 'calibrated' devices, but none use a standard, traceable method, partly due to the unavailability of such standards for measurements below 10 nN of force (Pratt et al. 2003).

Most researchers use a classical-theoretical approach to calibration by modeling their device as a linear elastic spring using:

$$F = kx \tag{1}$$

where F is the force, x is the displacement and k is the spring constant. Typically a device 'stiffness' is determined theoretically and displacements are taken from the device during the experiments. The force is then calculated using Eq. 1. This device stiffness, k, is a function of the elastic modulus and the geometry of the device. Yet, it is well known that these parameters are common sources of variation in flexible MEMS mechanisms (Mirfendereski et al. 1993). Furthermore, many researchers assume that the device geometry is well-defined. The device cross-section is usually assumed to be rectangular even though it is common knowledge that most fabrication processes involve etching steps that are notoriously asymmetric and introduce a significant

degree of taper that produces trapezoidal cross sections (Saif and McDonald 1998). Furthermore, elastic modulus values often quoted in the literature are typically that of the bulk material in a specific crystalline direction and in an undoped state. For example, consider a (100) wafer of single crystal silicon (SCS). Brantley (1973) showed that the elastic modulus of SCS lying in the 100 crystalline plane varies between 130.2 and 168.9 GPa dependent on orientation. Bhushan and Li (1997) showed that the elastic modulus of SCS can vary considerably depending on the level of doping.

When combined, these assumptions generate significant error in the force calculations. To add to the uncertainty, the derivation of the stiffness assumes that the device is behaving linearly, the deflections are small, the material is isotropic, etc. Add to this the fact that most MEMS processing routes generate significant residual stresses. These residual stresses can arise from thermal expansion mismatch of materials, doping, chemical machine polishing (CMP), etc. These are only a few examples of the processes that can affect the stress state of the structural material from which the MEMS device is fabricated. Clearly, these processes have changed the state of the material and changed the mechanical properties. It follows that this changes their mechanical response. Given the one-off nature of each MEMS device and the potential for great differences among ostensibly identical structures, it is crucial to develop a standard, post-fabrication calibration procedure, if such devices are to be used in making sensitive force measurements.

In this article, we present a simple technique for calibrating high-resolution load cells designed and fabricated in our lab. The proposed approach requires no assumptions of material properties or dimensions. We calibrate using a tried and true historical approach: by hanging dead weights, of precise magnitude, from our device. Though we applied this method to a specific load-cell design, it is clear that this is a general method applicable to nearly any MEMS configuration. We compare our calibrated force–displacement curves to a non-linear theoretical prediction, revealing errors as great as 29%.

2 Fabrication and characterization

2.1 Fabrication of the load cell

Load cells were fabricated using standard microprocessing techniques, consisting of a combination of vapor phase, wet, and dry etching. Fabrication began with an SOI wafer whose handle layer was 500 μm thick, a 2 μm thick buried oxide (BOX) layer, and a 20 μm thick device layer. All crystal orientations were (100). Fixed-fixed beam structures were then patterned using a layer of photoresist (PR). The device layer was then etched to the BOX layer by Deep Reactive Ion Etching (DRIE) of Si, using the Bosch (Lärmer and Schilp 1992) Process. Next, the remaining PR is removed using an O_2 plasma. The beams are then released using either an HF acid bath or vapor phase HF acid etch. The HF bath causes almost every structure to be stiction failed (Legtenberg et al. 1993) to the Si floor, thus a vapor phase HF etching apparatus was constructed to avoid this outcome (Fukuta et al. 2003). As a final step the handle layer of the wafer is removed from under the loading tip by cleavage. A schematic of the fabrication process is shown in Fig. 1.

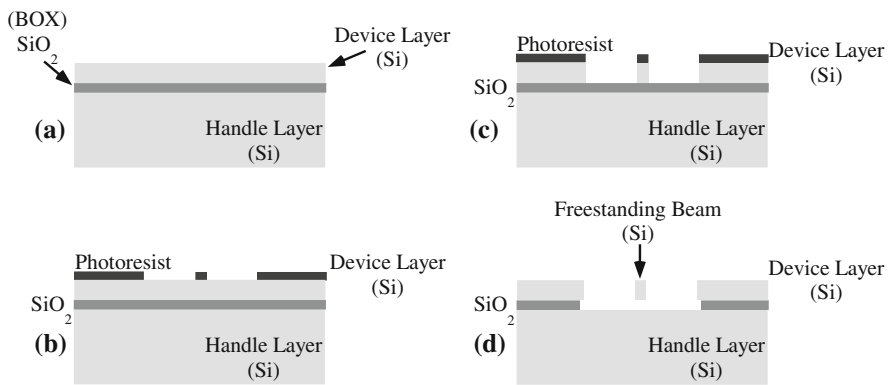

Fig. 1 Schematic of the fabrication steps used to produce the load cell: (**a**) Beginning substrate. (**b**) Photolithographic patterning. (**c**) Deep reactive ion etch of SCS using the Bosch (Lärmer and Schilp 1992) Process. (**d**) Removal of remaining photoresist (PR) and release using a vapor phase HF apparatus

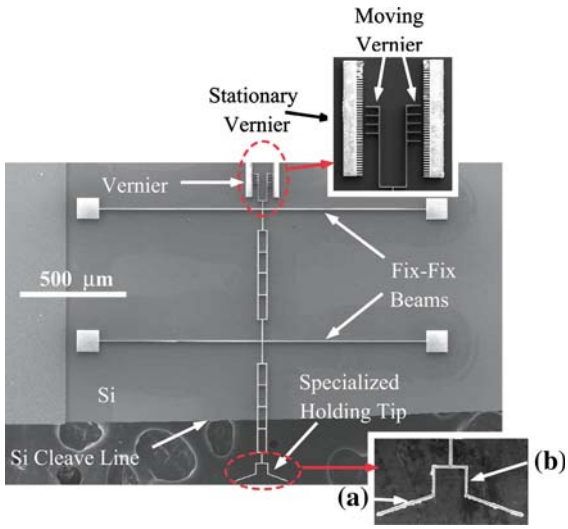

Fig. 2 An SEM image of a MEMS based load cell. This device consists of: SCS fixed-fixed beams (1,500 μm long), a vernier for measuring vertical displacements, and a testing tip where load is applied. (**a**) is an angled cantilever that was designed to be tangent to the surface of a 300 μm diameter sphere. (**b**) is a structure that allows for a controlled wicking of liquids

Figure 2 shows an SEM image of a typical load cell fabricated using the process described above. The lengths and widths are controlled by the dimensions set in the mask, while the depth of the structure (into the page) is set by the device layer's thickness. Any one of these dimensions can be changed in order to fine tune the desired stiffness. Thus far, devices have been fabricated successfully with stiffnesses, estimated using linear beam theory, between 1.74 and 376 nN/μm.

The load cell shown in Fig. 2 consists of two fixed-fixed beams joined at their center by a load transfer structure. A double fixed-fixed beam configuration was used to counteract any misalignments in the load tip and to limit rotations in and out of the plane of the load cell. Also attached at the center of the beams are two other devices. The one located at the top of the device is a vernier for measuring displacements to an uncertainty of 250 nm. At the bottom is a lamp-shade like structure that is used to attach a calibrated weight as well as a load tip. The angled cantilevers, labeled (a), will allow for more contact area between the calibration weight and load cell. The part labeled (b) is a structure that allows for a controlled wicking of adhesive or other liquids. The necessity for a wick-stop is described below.

2.2 Calibration procedure for the load cell

Calibration of the load cells is accomplished by hanging known weights from the portion of the load cell that extends beyond the cleave line of the wafer. After hanging the weight the deflection is recorded from the beam's vernier, Fig. 3. Hanging the weights, not surprisingly, requires extreme care. The weight is first properly aligned to the load cell using linear translation stages and goniometers. Weights were adhered to the load cell by using "secondary forces" and adhesives.

The calibration weights are commercially available sapphire ball lenses. These ball lenses are manufactured to tight specifications that allow great confidence in the weight of each sphere. The manufacturer's specification for density, ρ, is 3.98 ± 0.01 g/cm^3. Tolerances on all diameters was ± 2.54 μm. Independent verification was performed on several samples, through the use of a precision balance that is traceable to the National Institute of Standards and Technology (NIST), and it was found that all samples fall within the manufacturer's specifications.

To attain a centrally loaded fixed-fixed beam structure, proper alignment between the load cell and the ball lenses is necessary. This was accomplished through the use of three linear translation stages and two goniometers, see Fig. 4. The load cell was mounted onto a fixture that translates in the z-direction with goniometers that allow for rotation around the x and y-axes. The ball lenses were mounted onto a custom stage that allowed for the rigid temporary attachment of the ball lens to the x–y linear translation stages. The ball lenses are rigidly held in place by the application of a vacuum to the under side of the ball lens, upon adhesion of the ball lens to the load cell the vacuum was released. Upon proper alignment of the load cell and ball lens to gravity the ball lens was adhered to the load cell.

A non-linear force–displacement of the fixed-fixed beam structure was anticipated, thus a range of weights was hung from each load cell to capture the load cell's non-linear response. For ball lenses measuring, 300 and 500 μm in diameter, it was possible, when the humidity was relatively low, to attach the balls using static electricity. When the humidity was relatively high, it was possible to attach the balls using water menisci formed by the

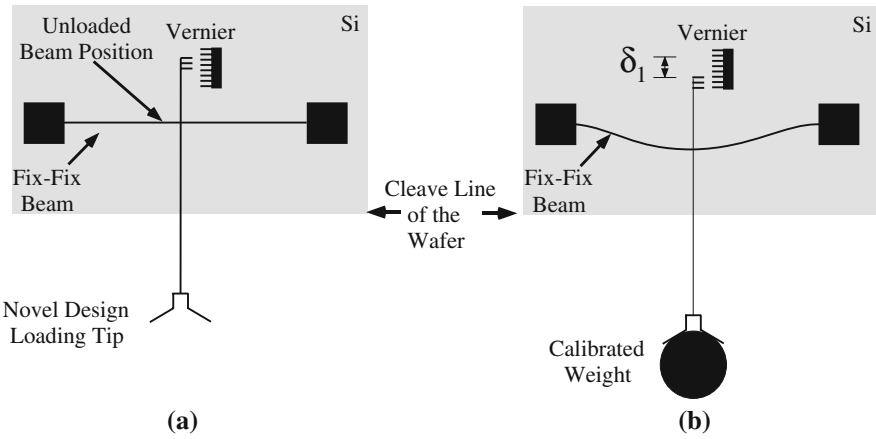

Fig. 3 Schematic of experimental setup showing the load cell: (**a**) Before hanging the calibration weight, and (**b**) after hanging the calibration weight

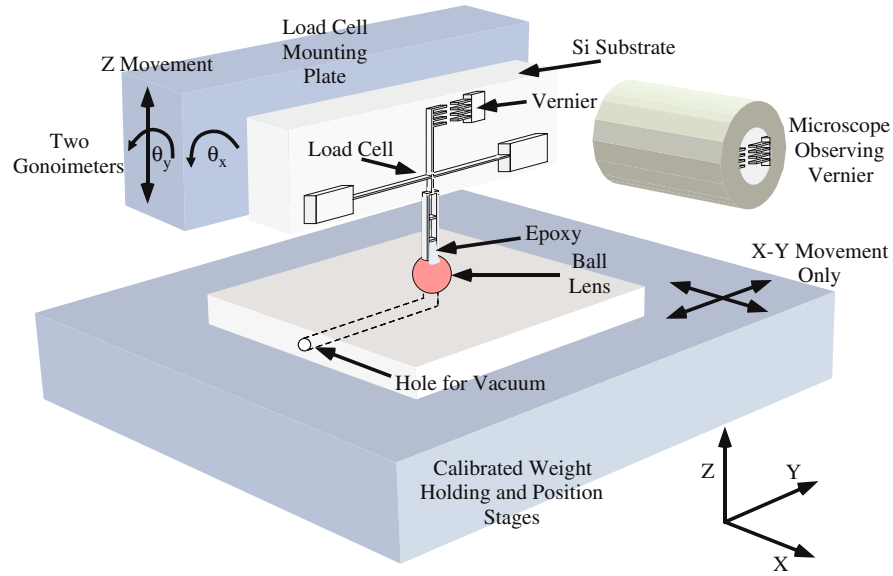

Fig. 4 Schematic of the experimental setup

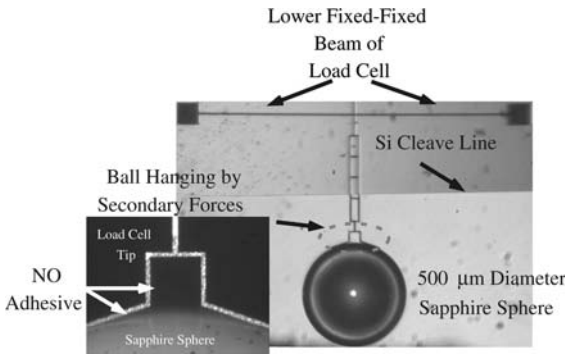

Fig. 5 A 500 μm diameter sapphire sphere attached to the tip of a load cell by secondary forces

condensed water from the humidity. Figure 5 shows an optical micrograph of a 500 μm sapphire ball lens attached in this manner to the load cell. Images of spheres attached by static electricity are similar. Detachment of these smaller spheres was possible through the use of surface tension. A droplet of water was placed onto a substrate and the sphere was brought near. When the sphere was placed into contact with the water, the water quickly pulled the ball from the load cell without damage.

At the extreme end of our load range the large diameter spheres were attached using an adhesive. Figure 6 shows an optical micrograph of a load cell terminated by a 1,000 μm diameter sphere. This sphere was attached by dipping the load cell's tip into a droplet of epoxy. The epoxy wicked into the load cell's specially designed 'lamp-shade' tip, this 'wet' tip was then lowered into contact with a large diameter sapphire sphere. It was possible to detach the spheres by vibrating the load cell. This was done

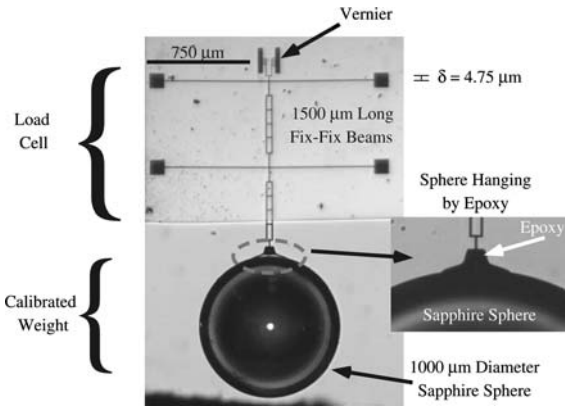

Fig. 6 A 1,000 µm diameter ball lens epoxied to the tip of the load cell

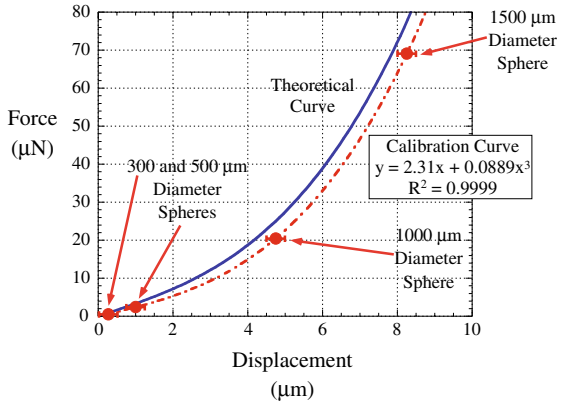

Fig. 7 Calibration curve for the load cell shown in Fig. 6

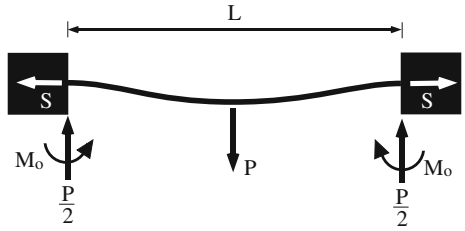

Fig. 8 Schematic of a centrally loaded fixed-fixed beam that develops an axial tensile force due to the beam's elongation

at some risk though, as some devices were damaged in this process. It should be noted at this point that the weight of the member from which the weights hang and the liquids used for attachment never total to greater than 0.1% of the minimum weight hung from the load cell. Therefore, this additional weight can be safely neglected.

The perils of removing the adhered sapphire balls prompted an alternate method of adhering larger sized ball lenses. Attachment of the load cell to a ball lens was possible using a positive photoresist. Solvents quickly escape the small volume of resist needed to adhere the ball lens to the load cell, especially under the intense light of the microscope. Removal of the ball lens and photoresist was performed by placing a dish of acetone under the load cell and ball lens assembly. The acetone vapor quickly weakens the positive photoresist because of the large dose of light it has received from the focused light of the microscope. Submersion of the ball lens and device was not necessary for ball lens removal.

2.3 Calibration data and analysis

Figure 7 shows a plot of an experimental calibration curve for the load cell shown in Fig. 6. Error bars for the displacement are due to reading of the vernier, and the error bars due to the uncertainty sphere weights are smaller than the data points themselves. The line to the left is the theoretical force–displacement curve, accounting for the nonlinear stiffening of a centrally loaded fixed-fixed beam [13]. Analyzing the beam, schematically illustrated in Fig. 8, yields the following equations:

$$\delta = 2\left(\frac{2I}{A_c}\right)^{\frac{1}{2}}(u - \tanh u)\left(\frac{3}{2} - \frac{1}{2}\tanh^2 u - \frac{3}{2}\frac{\tanh u}{u}\right)^{-\frac{1}{2}} \tag{2}$$

$$P = \frac{2EI}{L^3}\left(\frac{2I}{A_c}\right)^{\frac{1}{2}}u^3\left(\frac{3}{2} - \frac{1}{2}\tanh^2 u - \frac{3}{2}\frac{\tanh u}{u}\right)^{-\frac{1}{2}} \tag{3}$$

where,

$$u = \sqrt{\frac{SL^2}{EI}} \tag{4}$$

where δ is the lateral displacement of the midpoint of the fixed-fixed beam, I is the moment of inertia, A_c is the cross-sectional area of the beam, P is the lateral force applied at the midpoint of the beam, E is the elastic modulus, and L is the length of the beam. Simultaneous solution of Eqs. 2 and 3 are used to plot the theoretical line. In order to determine this theoretical curve it was necessary to use the SEM and precisely determine the dimensions of the load

cell's structure. The length, width, and height of the beams were found to be 1,500, 4.83, and 17.3 μm, respectively. We also assumed that the elastic modulus, E = 170 GPa because the beam is aligned to (110) plane. Theoretical predictions were quite close to the experimentally observed behavior of the beam, however, the experimentally measured displacements, for a given weight, are greater than predicted by the theory. This indicates that the beam is more compliant than predicted, likely due to an axial compressive force on the beam. This was verified by cofabricating beams of different length on the same die. Beams longer than 1,500 μm (including lengths of 3,000 and 5,000 μm) were all seen to buckle after release, indicating a compressive residual stress. Thus, the unbuckled shorter beams on the same die were expected to be more compliant due to the presence of a compressive axial load. Both curves were fitted using an equation of the form:

$$F = k_1 x + k_3 x^3 \tag{5}$$

where F is the central load on the beams, k_1 is the linear spring constant and k_3 is the cubic spring constant. The R^2 for the theoretical curve was 1 and for the experimentally measured curve it was 0.9999. Thus, an accurate calibration curve for this beam is possible only taking into account the cubic spring constant of the beam. This method has been successfully applied to several MEMS load cells similar to the one shown in Fig. 6.

Further scrutiny of Fig. 7 yields two other important observations. First, the linear range of the fixed-fixed beam extends only to about 1 μm, which is only one quarter of the width of the beam. Therefore, nonlinearities must be considered when analyzing fixed-fixed beams that have a relatively large deflection. Legtenberg and Elwenspoek (1996) arrived at a similar conclusion. Second, consider the amount of error between the theoretically predicted curve and calibration curve. Over the calibrated range, the percent error between the theoretically predicted curve and the calibration curve varies between 11 and 29%. Had careful characterization of the actuator not been undertaken in the SEM, this deviation could have been further augmented. Undoubtedly, elimination of the systematic error, due to lack of calibration, is necessary for the reporting of accurate results.

It is important to note that, due to the symmetric nature of the fixed-fixed beam in Fig. 2, the calibration range of the device can be doubled. In Fig. 9 let δ_1 be the deflection of the centerline of a fix-fix beam under the weight of the heaviest sphere. If an

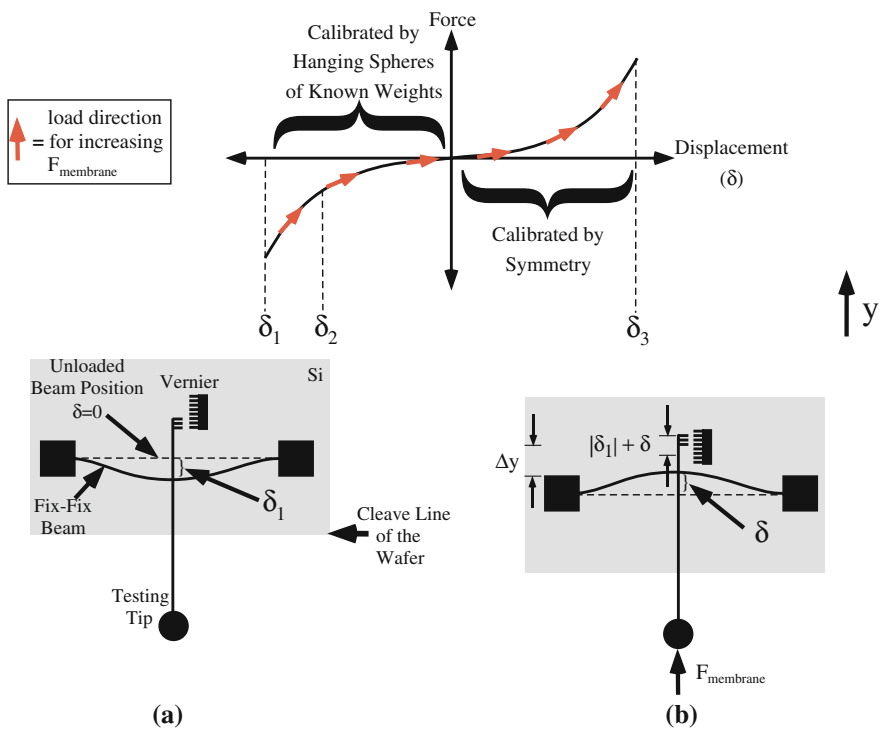

Fig. 9 Schematic of experimental setup. (**a**) Before loading and (**b**) after loading

assumption is made that the beam's response is symmetric, then one can assume that the beam is calibrated from δ_1 to δ_3 and of course $|\delta_1| = |\delta_3|$. If a lighter ball were attached to the load cell, then the initial deflection of the fixed-fixed beam might be δ_2. Then the beam can only have its centerline deflected from δ_2 to δ_3 and be in the calibrated region of the load cell. Thus, having the heaviest weight used for calibration still hanging from the load cell allows the load cell to be used across twice the range of calibration.

3 Summary

In this article we have demonstrated a novel method for the traceable calibration of MEMS devices by using the tried and true method of hanging calibrated dead weights. Here, traceability is attained by weighing of the weights on a NIST traceable precision scale. This method has been successfully applied to several MEMS devices in our laboratory. The methodology and specifics of interchanging and hanging the dead weights using surface tension of water, static electricity, epoxy and photoresist was described. A specific case was detailed, and it was shown that the nonlinear theoretical prediction of the load cell's response was in error, up to 29%, when compared to the calibrated response. These results show conclusively that accurate measurements require the calibration of individual load cells.

References

Bhushan, B., Li, X.: Micromechanical and tribological characterization of doped single-crystal silicon and polysilicon films for microelectromechanical systems devices. J. Mater. Res. **12**, 54–63 (1997)

Brantley, W.A.: Calculated elastic constants for stress problems associated with semiconductor devices. J. Appl. Phys. **44**, 534–535 (1973)

Frisch-Fay, R.: Flexible bars. Butterworths (1962)

Fukuta, Y., Fujita, H., Toshiyoski, H.: Vapor hydrofluoric acid sacrificial release technique for micro electro mechanical systems using labware. Jpn. J. Appl. Phys. **42**(6A), 3690–3694 (2003)

Lärmer, F., Schilp, A.: Method for anisotropically etching silicon. Patents DE4241045, US 5501893, and EP 625285 (1992)

Legtenberg, A.W.G.R., Elwenspoek, M.: Comb-drive actuators for large displacements. J. Micromech. Microeng. **6**, 320–329 (1996)

Legtenberg, R., Tilmans, A.C., Elders, J., Elwenspoek, M.: Stiction of surface microstructures after rinsing and drying: model and investigation of adhesion mechanisms. Sens. Actuators, Phys. A **43**, 230–238 (1993)

Mirfendereski, D., Lin, L., Kiureghian, A.D., Pisano, A.P.: Probabilistic response of micro-fabricated polysilicon beam structures: comparison of analysis and experiments. In: Dynamic Systems and Control Division, vol. 46. ASME (1993)

Onoe, Y., Takeo, T.: Probe-type microforce sensor for microactuators. In: Proceedings of SPIE – The International Society for Optical Engineering, vol. 3512, pp. 84–91 (1998)

Pratt, J.R., Newell, D.B., Kramar, J.A., Whitenton, E.: Calibration of piezoresistive cantilever force sensors using the NIST electrostatic force balance. In: Proceedings of IMECE'03, pp. 289–292. ASME, Washington, DC (2003)

Saif, M.T.A., MacDonald, N.: Measurement of forces and spring constants of microinstruments. Rev. Sci. Instrum. **69**(3), 1410–1422 (1998)

Samuel, B.A., Desai, A.V., Haque, M.A.: Microscale application of column theory for high resolution force and displacement sensing. Appl. Phys. Lett. **87**, 21904–1–3 (2005)

Sun, Y., Potasek, D.P., Piyabongkarn, D., Rajamani, R., Nelson, B.J.: Actively servoed multi-axis microforce sensors. In: International Conference on Robotics and Automation, pp. 294–299. IEEE, Taipei, Taiwan (2003)

Zhang, X.: Silicon microsurgery-force sensor based on optical MEMS encoders. Sensor Rev. **24**(1), 37–41 (2004)